



Limitations on maximum tree density using hyperspatial remote sensing and environmental gradient analysis

J.A. Greenberg^{a,*}, S.Z. Dobrowski^b, V.C. Vanderbilt^c

^a Center for Spatial Technologies and Remote Sensing (CSTARS), University of California, Davis, United States

^b Department of Forest Management, College of Forestry and Conservation, University of Montana, United States

^c NASA Ames Research Center, United States

ARTICLE INFO

Article history:

Received 28 September 2006

Received in revised form 17 July 2008

Accepted 24 August 2008

Keywords:

Environmental gradients

Ecological niche

Hyperspatial remote sensing

Topography

Radiation

Forests

Tree density

Lake Tahoe

ABSTRACT

We present a novel approach for performing environmental gradient analysis to address the question: is maximum potential tree density in eastern Lake Tahoe Basin, NV limited by water, temperature/energetic constraints, or both? To address this question we fuse continuous tree density estimates derived from hyperspatial remote sensing imagery (pixels smaller than trees) with two topographically derived environmental gradients: elevation and yearly potential relative radiation (PRR). We based our analysis on the maximum tree density found in each of over 200 environmental gradient combinations found with our area of interest, drawing from a dataset consisting of over 300,000 30 m plots and over 3 million individual trees. At a given elevation, sites in which maximum tree density increases as a function of increasing yearly PRR were considered to be temperature or energy limited. Conversely, sites in which maximum tree density decreased as a function of increasing yearly PRR were considered water limited. We found that eastern Lake Tahoe appears to be a landscape which is both water limited (at lower elevation and brighter, south-facing slopes) and temperature/energy limited (at higher elevations and darker, north-facing slopes). We discuss how fusing accurate and ecologically relevant remote sensing outputs with direct and indirect continuous microclimate surfaces can provide a powerful tool for addressing major questions of tree distributions and life history parameters.

© 2008 Published by Elsevier Inc.

1. Introduction

Alpine regions garner much attention due to the assumption that they will be “front line” indicators of large-scale shifts in ecosystem processes responding to changes in the climate (Grace et al., 2002; Hayhoe et al., 2004). Alpine forests grow to “treeline”, a spatially varying climatic limit (typically represented by an elevational threshold) above which trees, regardless of species, do not exist. Below treeline, tree spatial densities (number of trees per unit area) commonly decline with increasing elevation but mechanisms causing this decline are poorly understood and likely differ from site to site. Complicating the analysis is the fact that elevation is not the primary explanatory variable but is instead an indirect proxy variable. Increasing elevation is linked to increasing precipitation, decreased soil water holding capacity, decreasing temperature, and increasing solar irradiance (Urban et al., 2000). Even so, four primary mechanisms (Stevens & Fox, 1991; Körner, 1998) do appear important for explaining the tree density decrease with elevation: 1) frost damage, 2) insufficient available resources (water, light, carbon dioxide, nitrogen, other soil nutrients) to support minimum growth, 3) metabolic temperature requirements independent of

resource availability, and 4) disturbance from abiotic factors such as snow and ice, or biotic factors such as herbivores and pathogens.

Two general experimental approaches have investigated why tree density decreases with increasing elevation. Controlled experiments have quantified the response – tree establishment, growth and mortality – of potential causes (e.g. Handa et al., 2005). Gradient analysis (e.g. canonical correspondence analysis, Braak, 1986), used to infer those factors most related to tree density, has been applied to data collected from field plots or fossil records with known site conditions. Sampling issues limit the utility of both approaches. The design of the costly and time-consuming controlled experiments usually does allow control for site disturbance but generally is not able to control for other site conditions, which sometimes makes interpretation of results difficult. Conversely, the design of gradient analyses often does not allow the disentangling of complex interactions between variables related to site disturbance. For example, a site stem density may be low because the site has insufficient nutrients, water or light; because the site has experienced a recent disturbance; or because the site has avoided disturbance and has achieved a late-successional state characterized by low stem density – the “self thinning rule” (Westoby, 1984).

Here we present a third approach to understanding tree spatial density variation with elevation. Our approach analyzes climate limitations on tree distributions, drawing upon tree density estimates for contiguous plots that cover the landscape of interest overlaid upon environmental surfaces

* Corresponding author.

E-mail address: greenberg@ucdavis.edu (J.A. Greenberg).

derived from digital elevation models (DEMs) and micrometeorological modeling. To produce continuous data on vegetation characteristics, we employ individual tree crown mapping techniques applied to hyperspatial remotely sensed data (pixels smaller than the area of a tree crown). Tree crown mapping techniques have been developed for both optical data (e.g. Brandtberg & Walter, 1998; Gougeon, 1999; Pouliot et al., 2002; Leckie et al., 2003b; Greenberg et al., 2005a; Strand et al., 2006) and Lidar data (e.g. Brandtberg et al., 2003; Leckie et al., 2003a; Popescu et al., 2003; Falkowski et al., 2006), and has been demonstrated to be capable of producing accurate maps of per-tree positions, crown size, lifeform, species, leaf area index, and biomass. Our approach provides a *complete, spatially continuous* description of the tree density across a landscape at the 30 m scale and includes data layers describing local environmental and topographic conditions. Our approach, applied to the Lake Tahoe basin, provided over 300,000 sample plots, a number far exceeding that possible with traditional ground based methods. We examined multivariate predictors of tree density, removing the effects of site history by developing an analysis based upon the *maximum* tree density found for a given set of environmental conditions. This analysis has its roots in potential niche theory (Hutchinson, 1957) and bioclimate envelopes (Pearson & Dawson, 2003), focusing on maximum density of lifeforms (trees) rather than species.

Tree density is a function of the per-area probability that a tree can establish and avoid dying. Since we are unable to remotely sense small or understory trees, we modify this probability to include the probability that the tree will grow to a detectable size and remain in the canopy. Maximum possible tree density for given set of climatic conditions is likely to be found in recently disturbed, early successional forests. In the context of proposed treeline mechanisms, we examine whether maximum possible tree densities in eastern Lake Tahoe Basin controlled by water limitations or by factors related to temperature or energetic limitations (which could include insufficient photosynthetically active radiation, frost damage, or metabolic temperature requirements). To answer this, we make the following assumption: for all sites at a given elevation, convective temperature will be similar. The primary difference at sites at the same elevation, then, should be variations in solar irradiance due to aspect and slope differences. These differences in solar irradiance will: 1) increase plant metabolic temperatures in brighter sites, 2) increase photosynthetically active radiation (PAR) to plants in brighter sites, and 3) increase evaporative water loss from plants and the soil in brighter sites. This leads to the prediction that, at a given elevation, if a small, positive change in solar irradiance leads to an increase in maximum possible tree density, sites in this range of solar irradiance values are limited by temperature or energy since adding more solar

radiation increased the temperature and PAR and led to better conditions for trees. On the other hand, if a small, positive change in solar irradiance leads to a decrease in maximum possible tree density, sites in this range of solar irradiance are water limited since increased solar irradiance increased evaporative loss, and additional metabolic energy and PAR could not be used by the trees (e.g. Lloyd & Fastie, 2002). Fig. 1 illustrates this assertion. Qualitatively, we can state that the impact of climate change, specifically regional warming (with no change in precipitation), will negatively affect sites which are water limited, although we cannot predict increased tree densities from this analysis since we cannot detangle PAR vs. metabolic temperature limitations. Eastern Lake Tahoe has low annual actual evapotranspiration (Barbour et al., 2002), which is at the lower boundary of tree-dominated communities as described in Stephenson (1990), suggesting a largely water limited system. However, tree density declines precipitously at the higher elevations (Greenberg et al., 2005b), which is more indicative of a temperature-limited system (Paulsen et al., 2000). Indeed, the region may be limited by water in some locations, and temperature or energetics in others.

2. Methods

2.1. Site description

We analyzed data from an area of interest (“AOI”) located on the eastern shore of Lake Tahoe that spans the Nevada/California border. This AOI includes sections of the Carson and Sierra Nevada mountain ranges and spans elevations between 1900 m above sea level (asl) to 3400 masl. Vegetation communities are tree dominated (67% of the total cover) and shrub dominated (31% of the total cover), with *Pinus jeffreyi* (Jeffrey Pine), *Abies concolor* (White Fir) and *Abies magnifica* (Red Fir) dominated communities being the most common found in the Lake Tahoe Basin (Greenberg et al., 2006). Trees are found at nearly every elevation and exhibit a large range of tree densities. Two-thirds of the forests were clear-cut in the 19th century (Elliott-Fisk et al., 1997). Annually, the AOI receives on average 786 mm of precipitation in the form of rain or snow. Average daily temperatures range between -2°C in the winter to 13°C in the summer. The average number of frost-free days is 265 days. Average annual potential evapotranspiration calculated using the FAO Penman–Monteith methodology (Allen et al., 1998) is 1890 mm, with an average annual water deficit of 1104 mm (Dobrowski and Greenberg, unpublished data).

2.2. Imagery characteristics

IKONOS image data were acquired on 19 July 2002 covering our AOI. IKONOS collects 4 m multispectral data (blue, green, red and NIR bands), and 1 m panchromatic data. The imagery was atmospherically corrected, topographically flattened, calibrated with reference to ground spectra, orthorectified to approximately ± 5 m positional error and pansharpened using principal components pansharpening (Welch & Ehlers, 1987) to create a synthetic 4-band image, having 1 m pixels, that was used for all subsequent analyses. Greenberg et al. (2005a) describes the preprocessing of this dataset in more detail.

2.3. Tree crown detection and deriving tree density

We classified each pixel in the image as “shadowed vegetation,” “sunlit vegetation” and “other” with reference to thresholds: thresholds for shadowed vegetation pixels were red reflectance $< 4.2\%$ and normalized difference vegetation index (NDVI) ≥ 0.25 ; for sunlit vegetation, red reflectance $\geq 4.2\%$ and NDVI ≥ 0.25 ; for other, NDVI < 0.25 (Greenberg et al., 2005a). Based upon the classification results, we created for the AOI two masks representing sunlit and shadowed vegetation.

To detect all trees with radii R between $R_{\min} = 1$ m and $R_{\max} = 8$ m, we created a search algorithm, the “cross-shadow algorithm,” that applied a moving window filter to the two masks. At each window

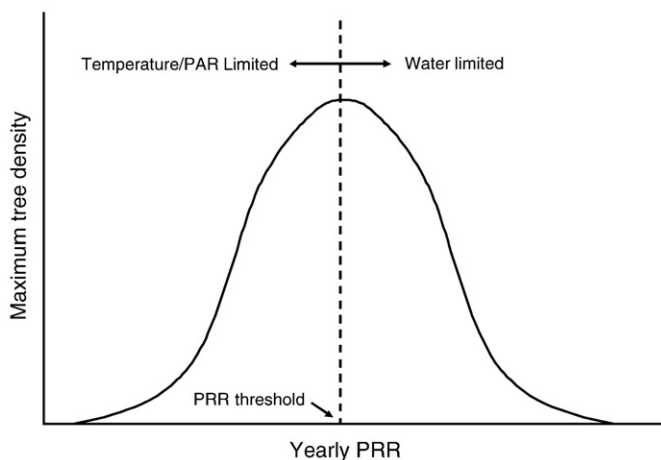


Fig. 1. For a given elevation range, we assert that regions with increasing maximum tree density with increasing yearly potential relative radiation (PRR) are limited by either metabolic temperature or photosynthetically active radiation (PAR). In regions with decreasing maximum tree density with increasing yearly PRR are likely to be water limited.

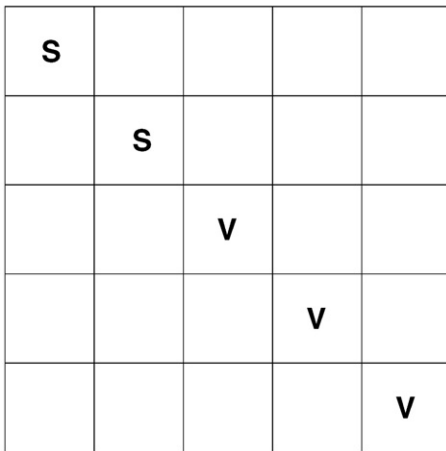


Fig. 2. Tree match filter for a tree with radius ~3 pixels and solar azimuth approximately 315°. The match is true if the underlying image window matches the shadowed vegetation pixels (S) and sunlit vegetation pixels (V). All blank cells in the filter are ignored.

location on the masks, the algorithm analyzed pixel values along a line in the principal plane (the plane defined by the two vectors that both originate at the center of the window and represent local Earth vertical and the local solar azimuth direction). The algorithm detected a candidate tree crown if, starting from window center, pixels on the line in the sunlit/shaded azimuth direction were classified as sunlit/shaded vegetation, respectively. The radius of the candidate tree crown was estimated from the maximum extent of the sunlit/shaded pixels from window center. Fig. 2 illustrates a sample filter for a tree radius of 3 pixels and a solar azimuth of 315°.

If a pixel is found to be a candidate tree crown, that pixel is given a value of the radius in pixel units plus a uniformly distributed random number u such that $0.0 < u < 1.0$. This resulted in one image per radius increment (candidate image identifiers are hereafter referred to as C_R , where R is the radius in pixels used to generate the candidate image). These images are then consolidated into a single image by taking the maximum value at any one location, e.g. the largest candidate found at a given location is selected, referred to as C_{max} , a single image containing, for each pixel, the largest radius plus random value found across all candidate images, C_R .

This image (C_{max}) will result in many more candidates than can realistically be found in a given location. One large tree crown is likely to contain multiple candidates, so we need to correct for these errors. We assume that no two trees can be closer than the larger of the two radii (e.g. the crowns can overlap with each other, but a tree's stem cannot overlap with the crown of another). In cases where trees do overlap significantly, we allow the larger of the two tree crowns to “trump” the

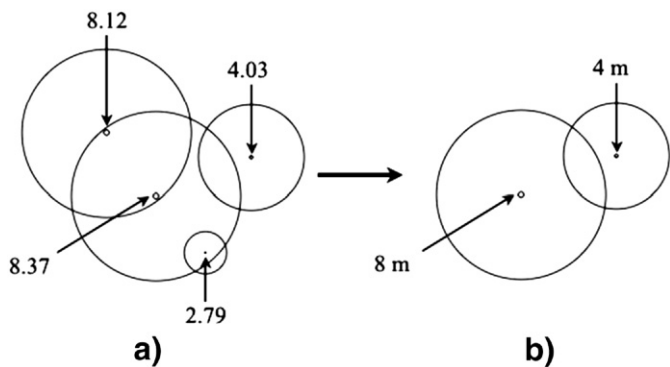


Fig. 3. Filtering process to remove overlapping crowns. (a) is an example of an output from choosing candidate tree sizes and centers. The values refer to the template size plus a random number between 0 and 1. (b) is the final output, where one of the two “tied” overlapping 8 m trees was eliminated by the random number, the 2 m tree was eliminated because it was smaller than the crown it fell within, and the 4 m tree was not eliminated because the stem did not fall within a larger tree's crown.

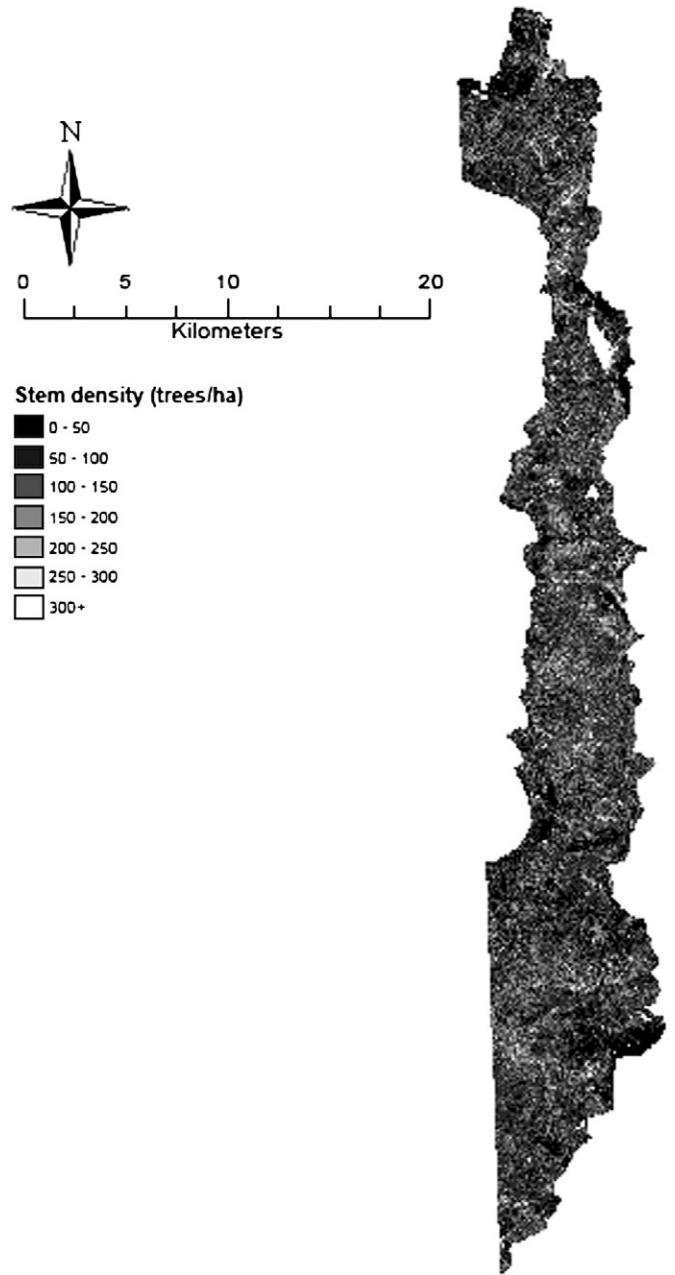


Fig. 4. Estimated stem density (trees/ha) derived from the cross-shadow tree crown mapping approach for eastern Lake Tahoe Basin.

smaller. In the case of two tree candidates being equally sized, we randomly choose one of the two tree candidates using the random values added to each radius. We illustrate the filtering process in Fig. 3. The iterative procedure for performing this analysis is as follows:

- 1) To begin, C_{max} is examined by passing a circular filter of radius R_{min} and checking for the maximum value in the filter at each pixel location. If the maximum value within this circular window equals the candidate value at that location (e.g. the center pixel has the maximum value of all candidates within the circle), the candidate value is written to an output file $O_{R_{min}}$, otherwise the output value at that location is 0.0.
- 2) For all remaining C_R such that $R_{min} < R \leq R_{max}$, we scan both O_{R-1} and C_{max} using a circular window of size R . If the maximum value in that circle equals the local C_R value, then O_R at that location is given the value of C_R , otherwise it is given the value of O_{R-1} .
- 3) A “floor” filter is applied to $O_{R_{max}}$ to remove the random decimals from the $O_{R_{max}}$ values. This results in a final “stem image” where pixel

values are 0 if there is no tree center present at that location, or >0 if there is a tree crown center. The integer values of the image are the predicted tree radius.

From our individual tree crown map, we derived stem density (trees/ha) by counting each stem falling in a 30 m area, and scaling to trees/ha. This resulted in a map of tree density for all of our AOI (Fig. 4). We note that the minimum possible tree size would have a crown radius of 1 m.

2.4. Accuracy assessment

We assessed the efficacy of the cross-shadow algorithm for detecting the presence/absence of trees in a given 30 m plot. We photointerpreted 50 randomly chosen 100 m × 100 m plots located in our imagery, correlating the photointerpreted stem densities and the stem densities predicted by the cross-shadow algorithm.

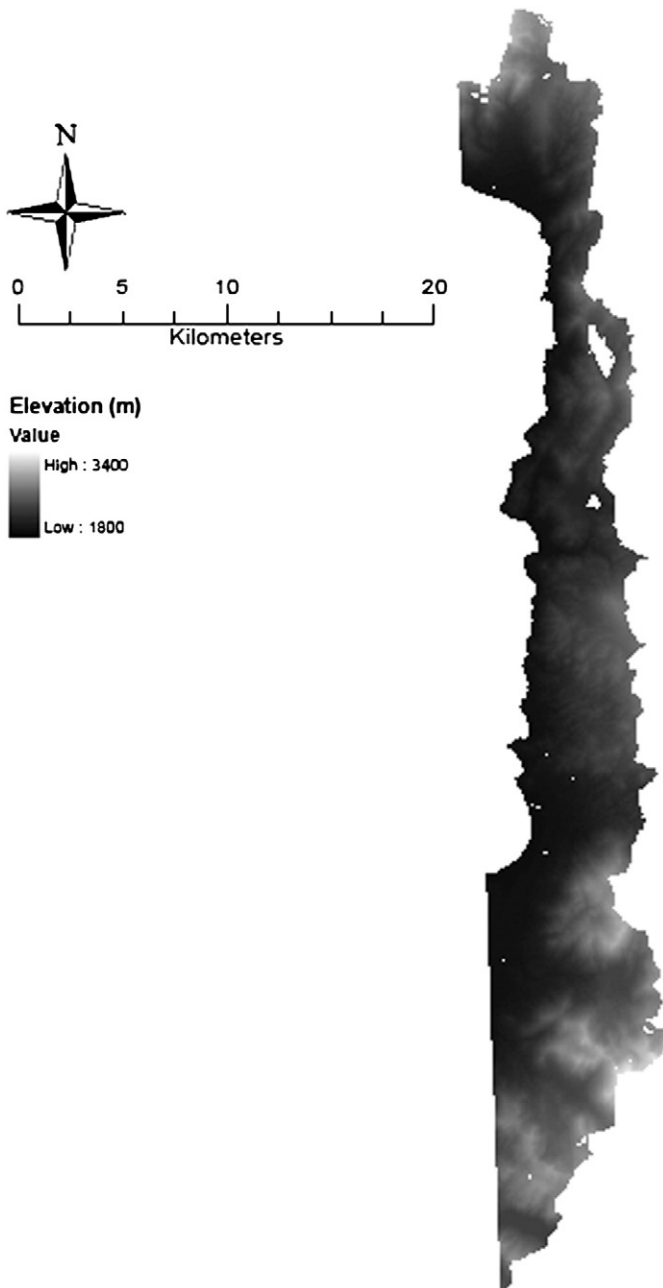


Fig. 5. Elevation (masl) for eastern Lake Tahoe Basin.

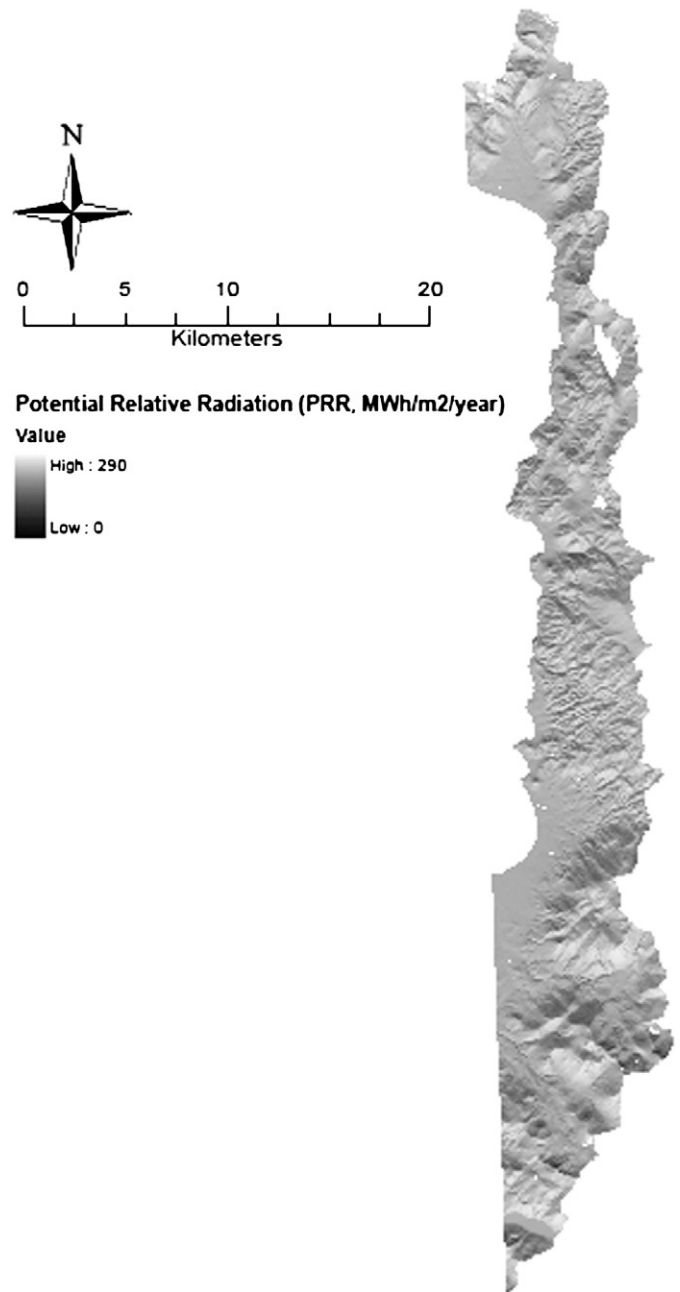


Fig. 6. Yearly potential relative radiation (PRR, MWh/m²/year) for eastern Lake Tahoe Basin.

2.5. Environmental gradients, gradient combinations, and continuous plots

We used two sets of topographically derived environmental gradients: elevation (Fig. 5) and yearly potential relative radiation (PRR, Fig. 6). We used the 30 m USGS DEM (U.S. Geological Survey, 1998) corresponding to the IKONOS scene to derive elevation (meters above sea level, masl) and to input into the potential relative radiation model. We used r.sun (Hofierka & Šúri, 2002) to predict clear-sky PRR across our area of interest. The model was used to simulate PRR on twelve days spaced evenly across the course of a year (one model run per month). The output of each individual run was multiplied by 30 to get the monthly PRR, and the twelve months then summed to get yearly PRR. We assume equivalent cloud conditions across our AOI, which means that yearly PRR should be directly related to cloud corrected yearly irradiance; we shall treat yearly PRR as a direct environmental variable for the purposes of this study.

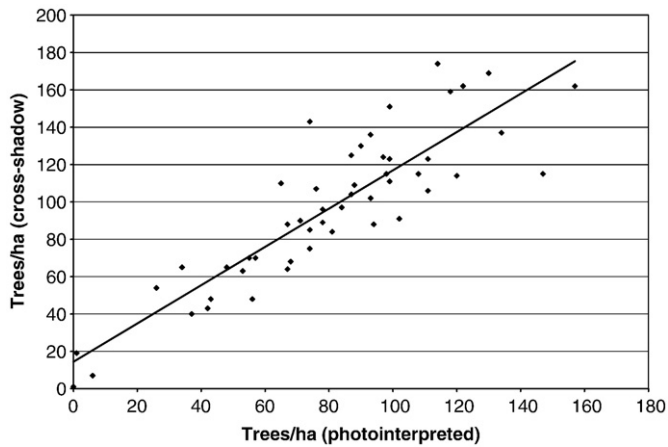


Fig. 7. Scatterplot of tree density estimated via cross-shadow algorithm vs. tree density estimated using photointerpretation stem count (photointerpreted) = $1.0247 * \text{stem count (cross-shadow)} + 14.437$ ($N=50$), with a correlation coefficient of 0.8773.

We divided our elevation surface into bins of 100 m (1800 m to 3300 m) and the yearly PRR surface into bins of 10 $\text{MWh/m}^2/\text{year}$ (range 0 $\text{MWh/m}^2/\text{year}$ to 290 $\text{MWh/m}^2/\text{year}$). Within the AOI, the 14 elevation bins \times 29 yearly PRR bins provide 406 possible “gradient combinations”, each a bivariate bin of elevation and yearly PRR. We overlaid the three data layers – representing each grid cell within the AOI, tree density, elevation bin, and yearly PRR bin – providing a contiguous, wall-to-wall map within the AOI of over 300,000 grid cells, hereafter referred to as “plots.”

2.6. Detecting maximum possible tree density and water limited sites

While, at a landscape scale, the Lake Tahoe Basin has been largely undisturbed since the clearcutting of the late 1800s (Elliott-Fisk et al., 1997), at a local scale individual plots will have a complex successional history and will, in most cases, lead to a sub-maximum tree density. We assume that sites which are at the maximum tree density are rare as a subset of all possible tree densities in a given gradient combination, so we only examined gradient combinations with a sufficient number of plots to accurately detect the upper bound of the distribution ($N \geq 50$ plots). For each gradient combination, we calculated the maximum stem density from the data. Additionally, for each elevation we determined the yearly PRR value at which the maximum stem density across all yearly PRR bins occurs (hereafter we will refer to this as the “PRR threshold”, see Fig. 1). Water limited sites, based on our assertions, are all sites at a given elevation which have PRR values above the PRR threshold for that elevation. Conversely, sites at a given elevation falling below the PRR threshold for that elevation are considered temperature or energetically limited. We used this threshold, in combination with the yearly PRR surface and the elevation surface to map water limited vs. temperature/energy limited sites.

3. Results

3.1. Tree crown detection

Comparing the photointerpreted versus predicted stem counts yielded a strong correlation coefficient of 0.8773 and a linear fit equation of:

$$\text{stem count (cross-shadow)} = 0.9759 * \text{stem count (photointerpreted)} + 14.089. \quad (1)$$

These results indicate that for tree density ranges in the Lake Tahoe Basin (0 to 150 trees/ha, Barbour et al., 2002), the cross-shadow

algorithm overestimates the tree density by between 14 trees/ha (at 0 trees/ha) and 18 trees/ha (at 150 trees/ha). We believe at least some of the bias error apparent in these results is attributable to the photointerpretation process. Fig. 7 shows the scatterplot of photointerpreted tree density vs. tree density estimated with the cross-shadow algorithm. Fig. 8a and b shows two examples of the tree crown identification outputs, one for a sparse shrub dominated alpine habitat, and one for a dense stand of smaller trees. Our analysis identified 3,102,601 trees in eastern Tahoe with a crown radius of at least 1 m.

3.2. Gradient combinations

In total, 336,815 plots, each $30 \text{ m} \times 30 \text{ m}$, were used in this analysis. The Forest Inventory and Analysis National Program, by comparison,

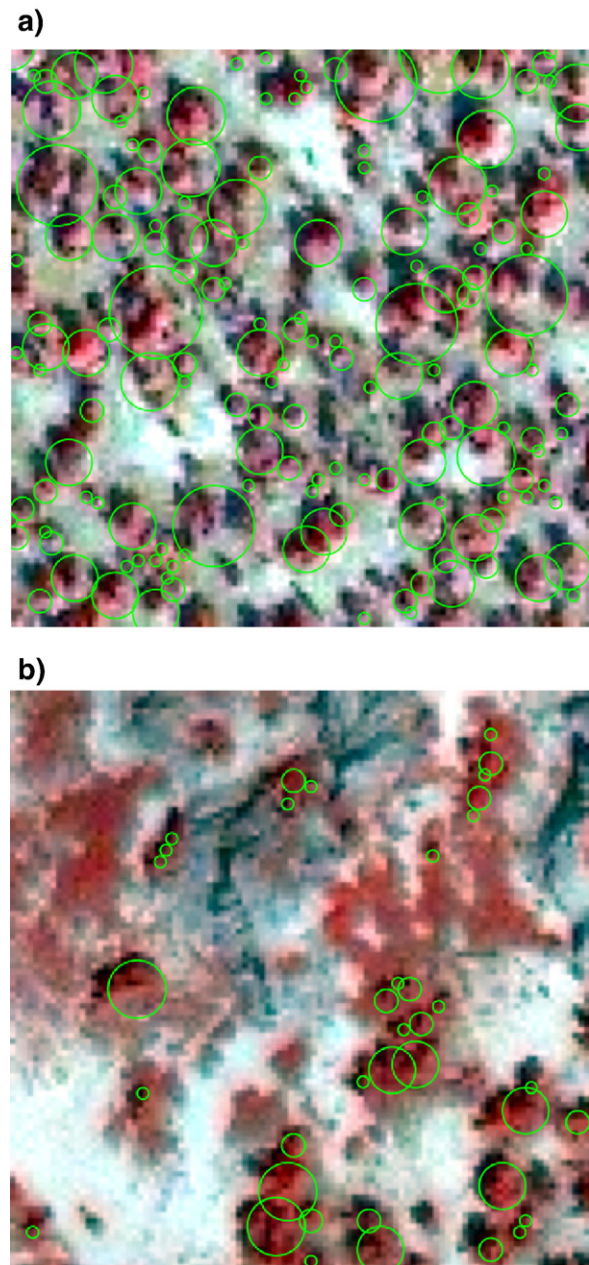


Fig. 8. Crown identification results for two selected plots. The background IKONOS images are false-color NIR (RGB=NIR, red, green). a) A dense stand of trees on a soil background (photointerpreted stem count 118, cross-shadow stem predicted stem count 159) and b) a sparse, shrub dominated region with shadow-casting rock formations (photointerpreted stem count 37, cross-shadow predicted stem count 40).

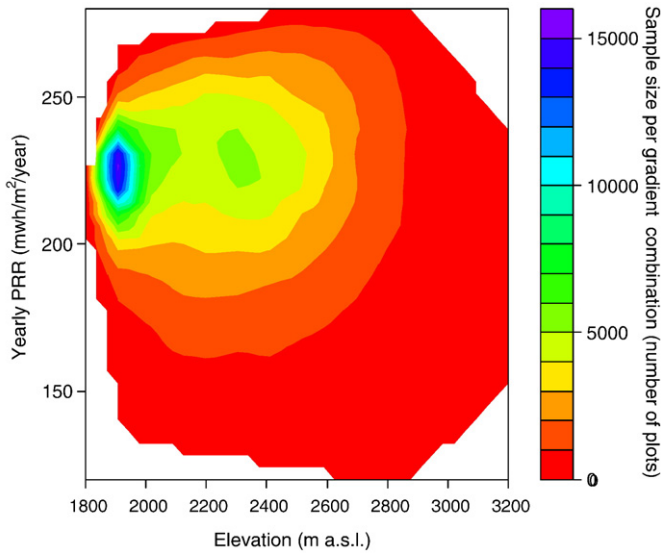


Fig. 9. Sample size (number of plots per gradient combination) as a function of elevation and yearly PRR bins.

has established 12 similarly sized plots to describe the same spatial extent (U.S. Department of Agriculture, 2003). Our AOI encompassed a total of 310 gradient combinations. Sample sizes per gradient combination ranged from 1 plot to 16,049 plots (mean 1086.5 plots per gradient combination). 213 of the 310 gradient combinations had sample sizes ≥ 50 plots. Gradient combinations with sufficient sample sizes ranged in elevation from 1800 m to 3200 masl, and ranged in yearly PRR from 120 MWh/m²/year to 280 MWh/m²/year. Fig. 9 displays the sample size of gradient combinations as a function of elevation and yearly PRR bin.

3.3. Maximum possible tree density

Fig. 10 displays the predicted maximum tree density of trees in eastern Lake Tahoe Basin. This graph shows a decidedly non-random distribution of values, with mid-range yearly PRR values (180 MWh/m²/year to 260 MWh/m²/year) having the highest maximum stem

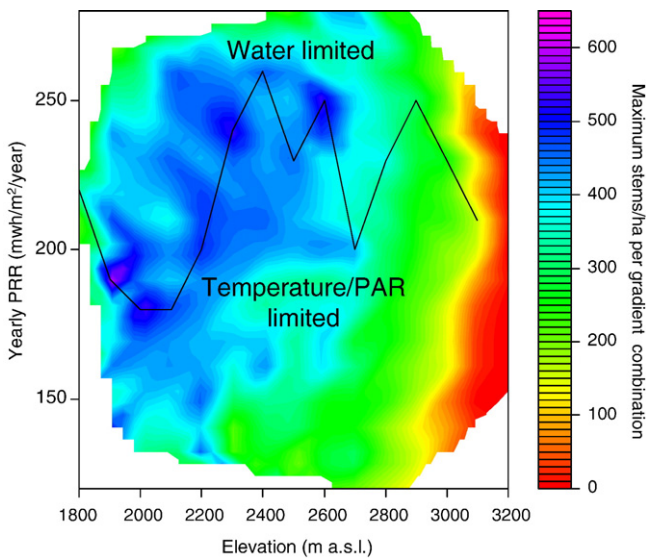


Fig. 10. Maximum tree density of trees as a function of environmental gradient combination in eastern Lake Tahoe Basin. Line demarcates the per elevation yearly PRR value for the peak tree density. Above this line, trees are water limited. Below this line, trees are temperature or PAR limited.

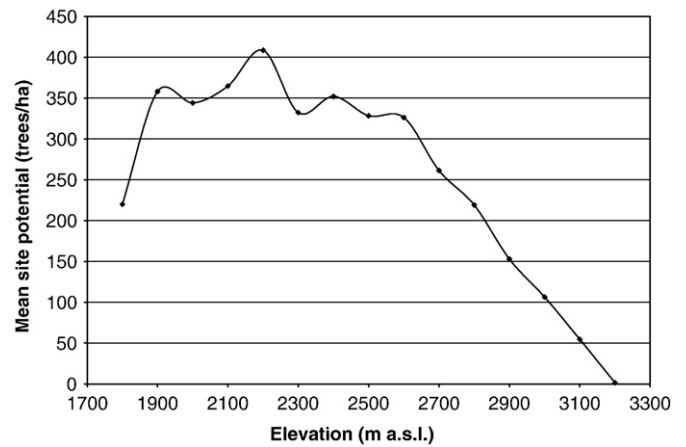


Fig. 11. Mean site potential (stems/ha) across all yearly PRR values as a function of elevation.

densities, and a generally decreasing maximum stem density as a function of elevation (see Fig. 11). The distribution of maximum stem density was unimodal at all elevations except for 3200 masl. The highest maximum stem density found in our AOI was 615 trees/ha, located in the 1900 masl and 190 MWh/m²/year bin. The lowest maximum stem density was 0, which we can classify as “tree line”, and was found in several gradient combinations at 3100 masl and a yearly PRR of 150 MWh/m²/year, and at 3200 masl at yearly PRR bins of 150 to 180, 200, and 220 to 240.

53% of the area in our AOI falls in regions where increasing PRR results in lower maximum stem density, and can be considered water limited (see Fig. 12 for a map of predicted water vs. energy limited regions for our AOI). Sites range from having 97% of the area in a given elevation range water limited (1900–2000 masl) to 26% of the area water limited (2600–2700 masl). Fig. 13 summarizes % water limitation by elevation.

4. Discussion

Maximum tree density within Eastern Lake Tahoe Basin appears to be driven by both water limitations (at lower elevations and in brighter, south-facing slopes) and temperature or PAR limitations (at higher elevations and in darker, north-facing slopes). These results underline the importance of a multivariate approach to analyzing vegetation response to environmental conditions: there is no landscape-wide, single limitation on trees in this region and tree density responses to climate change will be highly site-dependent. Maximum tree density in high radiation, low water environments is likely due to high seedling mortality (Germino et al., 2002). In sites found to be temperature or energetics limited, the possible mechanisms become more numerous. A longer duration of snowpack which occurs in colder sites reduces the growing season (Hansen-Bristow et al., 1988), colder sites will result in increased frost and other physical damage to the trees (Ives & Hansen-Bristow, 1983), and extremely low temperatures may restrict metabolic processes (e.g. Körner, 1998). Recent research has suggested future increased temperatures and lower precipitation in the Sierras Nevada as a consequence of increased atmospheric greenhouse gasses (Hayhoe et al., 2004). In water limited sites, increased yearly temperature and lowered precipitation will, in all likelihood, decrease maximum tree density and, overall, lower the mean tree density across the landscape (similar to results found in Lloyd and Fastie, 2002). In the temperature/energy limited sites, increased temperatures will likely increase stem density, as metabolic temperatures will increase, snow cover will decrease, and frost damage and other physical damage will decrease. However, temperature/energy limited sites which are near the PRR threshold will switch

to a water limited system, driving down maximum tree density at these sites.

This study illustrates the power of fusing remote sensing data with continuous coverages of environmental gradients for performing ecological gradient analysis. Hyperspatial optical data can be used to produce regional stem maps with a high degree of accuracy and high resolution DEMs can be used as a base for deriving environmental gradients at scales relevant to individual plants. Our data is the *population* of our AOI, not a sample, and we demonstrated how a dataset of this size can be used to analyze the extremes of a population of plants in a large number of gradient combinations. While we feel this analysis provides the basis of an important step towards vastly increasing our understanding of tree life history dynamics in the context of their local environment, this study is, in many ways, largely qualitative. The use of indirect variables such as elevation prevents direct quantification of effects of changing climate on stem density as well as our ability to

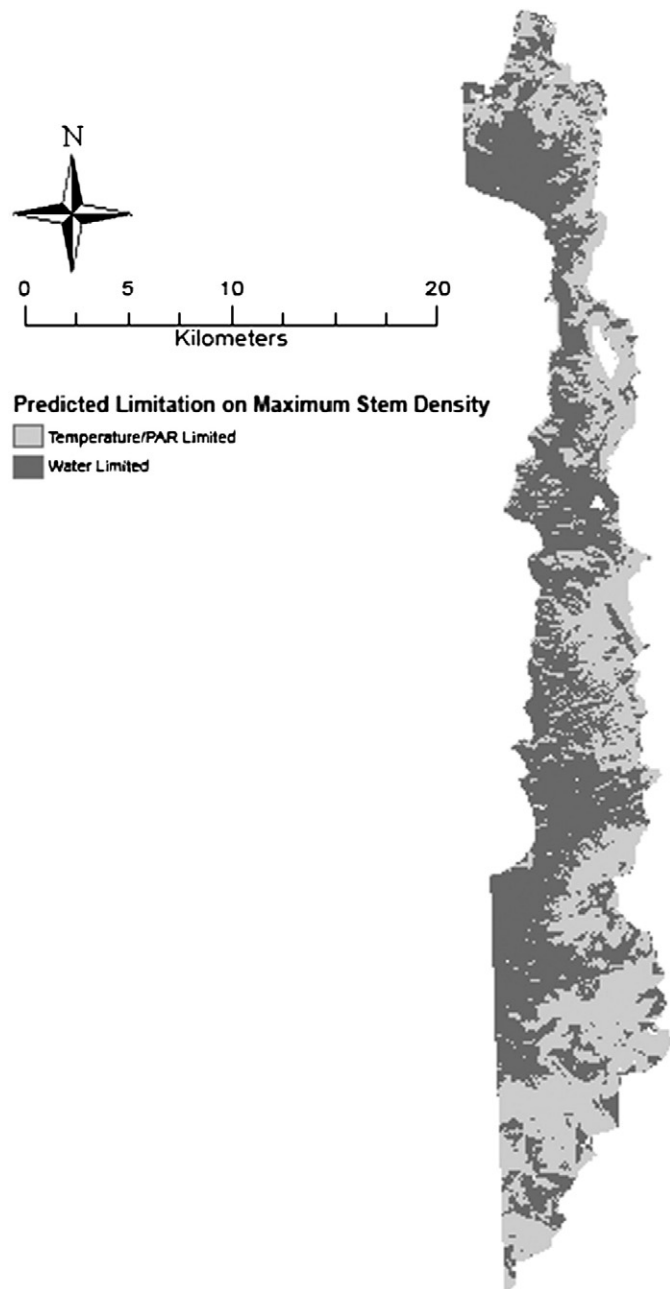


Fig. 12. Map of water limited regions vs. temperature/PAR limited regions for eastern Lake Tahoe Basin.

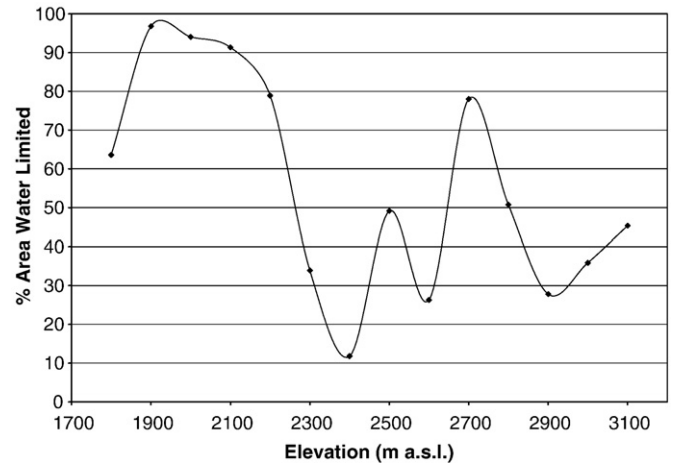


Fig. 13. % of area in a given elevation range that is predicted to be water limited (versus temperature or PAR limited).

predict stem density at other sites outside of the Basin. Major improvements to this type analysis will require the derivation and application of time specific microscale surfaces of factors which directly impact plant life history such as available water, wind speed, cloud- and vegetation-corrected PAR, air temperature, and annual snow cover, and to improve the derivation of tree types and state, including species, crown size and shape, and health. Improvements to the estimation of biophysical factors will require a combination of station data, mechanistic and empirical modeling, remote sensing products, and topographic information to generate (e.g. MTCLIM, Thornton & Running, 1999). Improvements to the estimation of tree types and state will require object-based, hyperspectral and/or Lidar analyses. Through these improvements, we can more specifically test hypotheses on the mechanisms of control of high elevation stem densities.

Producing primary data for ecological analyses from remotely sensed imagery requires outputs that are both accurate and relevant to testing major ecological theories. There has been an overemphasis in remote sensing on producing community-level maps despite the fact that using communities as the unit of ecological analysis has been largely discounted for over 60 years (Gleason, 1939). Additionally, certain biophysical variables such as leaf area index, biomass and carbon sequestration, which are useful in mechanistic models, have been repeatedly shown to be difficult to accurately map using coarse scale optical and RADAR techniques (Kasischke et al., 1997). The potential strengths of remote sensing, namely continuous characterization of a region and the enormous amount of data it can potentially produce, have been largely underutilized. Even situations in which outputs are both accurate and relevant (e.g. change detection results for deforestation), the size of the datasets has not often been leveraged to perform more complex multivariate analyses (but see Greenberg et al., 2005c). Hyperspatial optical and LIDAR image analysis techniques can produce relevant plant life history data at the scale of individual plants across extremely large regions. Advances in microclimate can allow us to produce the “physical template” (Urban et al., 2000) in which to examine plant life history. By fusing the two, there is the potential for an important expansion in our understanding of plant responses to climate change across regional or continental scales.

References

- Allen, R. G., Pereira, L. S., Raes, D., & Smith, M. (1998). *Crop evapotranspiration-Guidelines for computing crop water requirements-FAO Irrigation and drainage paper 56* (pp. 300). Rome: FAO.
- Barbour, M., Kelley, E., Maloney, P., Rizzo, D., Royce, E., & Fites-Kaufmann, J. (2002). Present and past old-growth forests of the Lake Tahoe Basin, Sierra Nevada, US. *Journal of Vegetation Science*, 13, 461–472.
- Braak, C. (1986). Canonical correspondence analysis: A new eigenvector technique for multivariate direct gradient analysis. *Ecology*, 67, 1167–1179.

- Brandtberg, T., & Walter, F. (1998). Automated delineation of individual tree crowns in high spatial resolution aerial images by multiple-scale analysis. *Machine Vision and Applications*, 11, 64–73.
- Brandtberg, T., Warner, T. A., Landenberger, R. E., & McGraw, J. B. (2003). Detection and analysis of individual leaf-off tree crowns in small footprint, high sampling density lidar data from the eastern deciduous forest in North America. *Remote Sensing of Environment*, 85(3), 290–303.
- Elliott-Fisk, D. L., Cahill, T. C., Davis, O. K., Duan, L., Goldman, C. R., Gruell, G. E., Harris, R., Kattelmann, R., Lacey, R., & Leisz, D. (1997). Lake Tahoe case study. *Sierra Nevada Ecosystem Project: Final Report to Congress Addendum*. (pp. 217–276).
- Falkowski, M. J., Smith, A. M. S., Hudak, A. T., Gessler, P. E., Vierling, L. A., & Crookston, N. L. (2006). Automated estimation of individual conifer tree height and crown diameter via two-dimensional spatial wavelet analysis of lidar data. *Canadian Journal of Remote Sensing*, 32, 153–161.
- Germino, M. J., Smith, W. K., & Resor, A. C. (2002). Conifer seedling distribution and survival in an alpine-treeline ecotone. *Plant Ecology*, 162, 157–168.
- Gleason, H. A. (1939). The individualistic concept of the plant association. *American Midland Naturalist*, 21, 92–110.
- Gougeon, F.A., 1999. Automatic individual tree crown delineation using a valley-following algorithm and a rule-based system. Pages 11–23 in Hill, D.A. and Leckie, D.G., editors. International Forum on Automated Interpretation of High Spatial Resolution Digital Imagery for Forestry. Natural Resources Canada, Canadian Forest Service, Victoria, B.C.
- Grace, J., Berninger, F., & Nagy, L. (2002). Impacts of climate change on the tree line. *Annals of Botany (London)*, 90(4), 537–544.
- Greenberg, J. A., Dobrowski, S. Z., Ramirez, C. M., Tuil, J. L., & Ustin, S. L. (2006). A bottom-up approach to vegetation mapping of the Lake Tahoe Basin using hyperspatial image analysis. *Photogrammetric Engineering & Remote Sensing*, 72, 581–589.
- Greenberg, J. A., Dobrowski, S. Z., & Ustin, S. L. (2005). Shadow allometry: Estimating tree structural parameters using hyperspatial image analysis. *Remote Sensing of Environment*, 97, 15–25.
- Greenberg, J. A., Dobrowski, S. Z., & Vanderbilt, V. C. (2005). Evidence of water limited affects in tree density in a subalpine/alpine environment as inferred from hyperspatial image data and climate gradient analysis. *American Geophysical Union Fall Meeting San Francisco, CA*.
- Greenberg, J. A., Kefauver, S. C., Stimson, H. C., Yeaton, C. J., & Ustin, S. L. (2005). Survival analysis of a neotropical rainforest using multitemporal satellite imagery. *Remote Sensing of Environment*, 96, 202–211.
- Handa, I. T., Körner, C., & Hättenschwiler, S. (2005). A test of the treeline carbon limitation hypothesis by in situ CO₂ enrichment and defoliation. *Ecology*, 86, 1288–1300.
- Hansen-Bristow, K. J., Ives, J. D., & Wilson, J. P. (1988). Climatic variability and tree response within the forest-alpine tundra ecotone. *Annals of the Association of American Geographers*, 78(3), 505–519.
- Hayhoe, K., Cayan, D., Field, C. B., Frumhoff, P. C., Maurer, E. P., Miller, N. L., Moser, S. C., Schneider, S. H., Cahill, K. N., & Cleland, E. E. (2004). Emissions pathways, climate change, and impacts on California. *Proceedings of the National Academy of Sciences*, 101, 12422–12427.
- Hofierka, J., & Šúri, M. (2002). The solar radiation model for open source GIS: Implementation and applications. *Proceeding of Open Source GIS-GRASS Users Conference*.
- Hutchinson, G. E. (1957). Concluding remarks. *Cold Spring Harbor Symposia on Quantitative Biology*, 22, 415–427.
- Ives, J. D., & Hansen-Bristow, K. J. (1983). Stability and instability of natural and modified upper timberline landscapes in the Colorado Rocky Mountains, USA. *Mountain Research and Development*, 3(2), 149–155.
- Kasischke, E. S., Melack, J. M., & Dobson, M. C. (1997). The use of imaging radars for ecological applications – A review. *Remote Sensing of Environment*, 59, 141–156.
- Körner, C. V. (1998). A re-assessment of high elevation treeline positions and their explanation. *Oecologia*, 115, 445–459.
- Leckie, D., Gougeon, F., Hill, D., Quinn, R., Armstrong, L., & Shreenan, R. (2003). Combined high-density lidar and multispectral imagery for individual tree crown analysis. *Canadian Journal of Remote Sensing*, 29, 633–649.
- Leckie, D. G., Gougeon, F. A., Walsworth, N., & Paradine, D. (2003). Stand delineation and composition estimation using semi-automated individual tree crown analysis. *Remote Sensing of Environment*, 85(3), 355–369.
- Lloyd, A. H. N., & Fastie, C. L. N. (2002). Spatial and temporal variability in the growth and climate response of treeline trees in Alaska. *Climatic Change*, 52, 481–509.
- Paulsen, J., Weber, U. M., & Koerner, C. (2000). Tree growth near treeline: Abrupt or gradual reduction with altitude? *Arctic, Antarctic, and Alpine Research*, 32, 14–20.
- Pearson, R. G., & Dawson, T. P. (2003). Predicting the impacts of climate change on the distribution of species: Are bioclimate envelope models useful? *Global Ecology and Biogeography*, 12, 361–371.
- Popescu, S. C., Wynne, R. H., & Nelson, R. F. (2003). Measuring individual tree crown diameter with lidar and assessing its influence on estimating forest volume and biomass. *Canadian Journal of Remote Sensing*, 29, 564–577.
- Pouliot, D. A., King, D. J., Bell, F. W., & Pitt, D. G. (2002). Automated tree crown detection and delineation in high-resolution digital camera imagery of coniferous forest regeneration. *Remote Sensing of Environment*, 82, 322–334.
- Stephenson, N. L. (1990). Climatic control of vegetation distribution: The role of the water balance. *American Naturalist AMNTA*, 4, 135.
- Stevens, G. C., & Fox, J. F. (1991). The causes of treeline. *Annual Review of Ecology and Systematics*, 22, 177–191.
- Strand, E. K., Smith, A. M. S., Bunting, S. C., Vierling, L. A., Hann, D. B., & Gessler, P. E. (2006). Wavelet estimation of plant spatial patterns in multitemporal aerial photography. *International Journal of Remote Sensing*, 27, 2049–2054.
- Thornton, P. E., & Running, S. W. (1999). An improved algorithm for estimating incident daily solar radiation from measurements of temperature, humidity, and precipitation. *Agricultural and Forest Meteorology*, 93, 211–228.
- Urban, D. L., Miller, C., Halpin, P. N., & Stephenson, N. L. (2000). Forest gradient response in Sierran landscapes: The physical template. *Landscape Ecology*, 15, 603–620.
- U.S. Department of Agriculture, F. S. (2003). Forest inventory and analysis national core field guide, volume 1: Field data collection procedures for phase 2 plots, version 1.7. *U.S. Department of Agriculture, Forest Service Washington: Washington Office*.
- U.S. Geological Survey (1998). *7.5 minute Digital Elevation Models* Menlo Park: U. S. Geological Survey.
- Welch, R., & Ehlers, M. (1987). Merging multiresolution SPOT HRV and Landsat TM data. *Photogrammetric Engineering and Remote Sensing*, 53, 301–303.
- Westoby, M. (1984). The self-thinning rule. *Advances in Ecological Research*, 14, 167–226.